Vol. 685: 69–84, 2022
https://doi.org/10.3354/meps13979

MARINE ECOLOGY PROGRESS SERIES
Mar Ecol Prog Ser

Published March 10

Singularities of surface mixing activity in the Western Mediterranean influence bluefin tuna larval habitats

L. Díaz-Barroso[1,*], I. Hernández-Carrasco[1,2], A. Orfila[2], P. Reglero[3], R. Balbín[3], M. Hidalgo[3], J. Tintoré[1,2], F. Alemany[3,4], D. Alvarez-Berastegui[3]

[1]SOCIB, Balearic Islands Coastal Observing and Forecasting System, 07122 Palma de Mallorca, Spain
[2]IMEDEA (CSIC-UIB), Institut Mediterrani d'Estudis Avançats, 07190 Esporles, Spain
[3]CN-IEO-CSIC, Instituto Español de Oceanografía, Centre Oceanogràfic de les Balears, 07015 Palma de Mallorca, Spain
[4]ICCAT, International Commission for the Conservation of Atlantic Tunas, 28002 Madrid, Spain

ABSTRACT: Understanding how the surface dynamics of the ocean influence the spawning and larval ecology of many large pelagic species, in particular tuna species, is a major challenge. For temperate tunas, the selection of geographically restricted spawning grounds is influenced by environmental conditions, but the influence of surface mixing properties on the early life stages of these species remains poorly understood. Here, based on ichthyoplankton samples collected over 4 yr and satellite-derived finite size Lyapunov exponents (FSLEs), we examined how horizontal mixing activity drives the probability of presence of Atlantic bluefin tuna *Thunnus thynnus* larvae. We further analyzed the spatial and temporal scales of the FSLE variability at which the relationship between larval presence and mesoscale activity is maximized. We found that moderate mixing activity strongly favors the spatial–temporal distribution of larval habitats, evidencing an optimal environmental window of bluefin tuna spawning and early life development within the mesoscale dynamics. During the spawning season, the Balearic Sea presents a unique spatial and temporal hydrodynamic scenario within the Western Mediterranean. These results can be used for developing oceanographic indicators and improving larval abundance indices that are currently used in Atlantic bluefin tuna stock assessments.

KEY WORDS: Finite size Lyapunov exponents · Mixing activity · Early life ecology · *Thunnus thynnus* · Optimal environmental window · OEW · Seascape ecology · Balearic Sea

1. INTRODUCTION

Tuna species with restricted spawning grounds travel long distances from the foraging areas to reach geographical locations with particular environmental conditions that may favor the survival and growth of early life stages (Muhling et al. 2013, Ciannelli et al. 2015). This is the case for Atlantic bluefin tuna *Thunnus thynnus* that spends most of its annual cycle in productive regions of the North Atlantic and other areas, but in the beginning of spring travels long distances to aggregate in particular reproductive areas. Understanding the reasons for the selection of specific areas for reproduction is one main focus of researchers investigating the ecology of this emblematic species, which also has implications for its adequate management (Porch et al. 2019).

One key approach is to identify the particular environmental characteristics that make these spawning regions adequate for the early life stages of this species. The characterization of these environmental particularities is relevant from 2 different perspectives. Firstly, it identifies cues related to ecological processes behind the selection of these reproductive

*Corresponding author: lara.diaz.barroso@gmail.com

Publisher: Inter-Research · www.int-res.com

areas, and secondly, it allows the design of ocean indicators used to properly monitor interannual changes potentially affecting the species of interest. Previous studies within the Balearic Sea (Western Mediterranean), one of the most relevant spawning grounds of bluefin tuna (Rooker et al. 2007, Alemany et al. 2010), have shown that during the spawning season these areas present temperature ranges favoring egg survival and larval growth (Reglero et al. 2018), low levels of primary production (Alvarez-Berastegui et al. 2016, Druon et al. 2016), association with the presence of oceanic density fronts (Alvarez-Berastegui et al. 2014) and a spatial–temporal segregation with main predators such *Pelagia noctiluca* ephyrae (Ottmann et al. 2021). Some of these characteristics are similar in other important spawning grounds (Muhling et al. 2017).

Recent research highlights the need to consider the environmental drivers influencing distribution and production of marine resources across life stages and spatial scales (Twiname et al. 2020), which are highly relevant for spawning and early life survival of tuna species. The integration of information relating the ecology of the bluefin tuna to environmental variability has had a positive impact on the estimation of different parameters used for fisheries assessment processes (Ingram et al. 2017, Reglero et al. 2019, Alvarez-Berastegui 2020). However, there are still different aspects of the local mesoscale oceanography that could play a key role in defining the optimal environmental window (OEW; Cury & Roy 1989) that characterizes spawning and larval survival of the Atlantic bluefin tuna that have not yet been studied and that could provide valuable knowledge for understanding the clues that make this species select specific areas as spawning grounds. This is the case with the surface mixing associated with surface hydrodynamic processes.

Previous studies investigating how oceanographic processes determine the habitats of bluefin larvae have inferred and parameterized the mesoscale activity through eddy kinetic energy (EKE) (Alvarez-Berastegui et al. 2016) or geostrophic velocity (GVEL) (Alemany et al. 2010, Reglero et al. 2012, Alvarez-Berastegui et al. 2014), which are Eulerian diagnoses based on the analysis of snapshots of velocity fields at given time. However, the development over the last decade of new techniques from a Lagrangian perspective has provided new opportunities to analyze transport properties in turbulent flows. While the Eulerian diagnosis only describes the spatial characteristics of the currents, in the Lagrangian perspective, both temporal and spatial variability of the velocity field are explored through fluid particle trajectories, allowing measuring the effects on transport of this velocity field. In particular, finite size Lyapunov exponents (FSLEs) (Aurell et al. 1997, d'Ovidio et al. 2004), based on the separation rate of a pair of particle trajectories, provide additional and complementary information for the most common Eulerian approaches in the analysis of the mixing mechanisms of water masses (d'Ovidio et al. 2009, Hernández-Carrasco et al. 2012). Unlike GVEL or EKE, FSLEs provide information of the sea surface mixing dynamics at smaller scales than the velocity field resolution (i.e. sub-grid filaments), generated by the interaction of oceanographic structures occurring at larger scales, i.e. mesoscale eddies or fronts (Hernández-Carrasco et al. 2011, Hernández-Carrasco & Orfila 2018). The advantages and potential of FSLEs for investigating the relations between physical and ecological interactions in the pelagic realm have emerged in the last decade. Some examples are the application of FSLEs for understanding the effects of lateral advection on the dynamics of sea surface temperature and chlorophyll *a* filaments observed in satellite images (Lehahn et al. 2007, Hernández-Carrasco et al. 2018), with direct impact on the intermediate trophic levels (Maps et al. 2015) and megafauna behavior (Tew Kai et al. 2009, Abrahms et al. 2018, Scales et al. 2018). Within the Balearic Sea, FSLEs have been used to investigate the effects of surface mixing induced by eddy–eddy interactions on phytoplankton dynamics (Hernández-Carrasco et al. 2020).

In this work, we investigated how sea surface mixing, derived from mesoscale activity, helps to characterize bluefin tuna larval habitats in the Balearic Sea. We focused on analyzing the existence of a relationship between Lagrangian measures of horizontal mixing intensity, parameterized by FSLEs, and the presence of bluefin tuna larvae. We also identified the most adequate spatial scale at which integration of FSLE values maximizes the probability of identifying larval habitats from satellite altimetry. We then explored the spatial and temporal particularities that the mixing activity presents in the bluefin tuna spawning area, comparing regional and seasonal differences in FSLEs over the Western Mediterranean basin. This allowed us to identify environmental characteristics selected by bluefin tuna for reproduction, as well as to develop remote sensing based monitoring indicators of the environmental variability affecting the ecology of this emblematic species, facilitating the integration of environmental variability in fisheries assessment processes.

2. MATERIALS AND METHODS

2.1. Study area and *in situ* sampling

The study area is located around the Balearic archipelago (box B in Fig. 1), covering the most relevant spawning grounds of Atlantic bluefin tuna in the Western Mediterranean Sea). This area is characterized by 2 separate regions with different water masses: cooler and more saline resident Mediterranean waters in the north and warmer and fresher Atlantic waters in the south (Sayol et al. 2013, Hernández-Carrasco et al. 2020). The Balearic and Algerian basins are connected by the Balearic Channels (Ibiza Channel, Mallorca Channel and Menorca Channel), with complex bathymetry around the islands. The Western Mediterranean shows strong mesoscale activity and a general circulation pattern that is highly variable by year and seasonal temporal scales (Pinot et al. 1994, 1995, 2002). In the northwestern Mediterranean, the Northern Current (Fig. 1, box A) flows southward along the Spanish shelf-slope. Part of the Northern Current crosses the Balearic basin through the Ibiza Channel, while the other part is deflected eastward, forming the Balearic Current (La Violette et al. 1990, Salat 1995, García-Ladona et al. 1996). Also, around the Balearic Islands, a salinity-driven front characterizes the mesoscale oceanography patterns of the bluefin tuna spawning grounds during the spawning season (Balbín et al. 2014). In the southwestern region, the average circulation is dominated by the Algerian Current (Fig. 1, box C) and a large number of front and eddy structures induced by the interaction of this boundary current with the steep coastal topographic slopes (Escudier et al. 2016, Capó et al. 2019).

Six oceanographic cruises were carried out between 2011 and 2014, sampling a grid of stations distributed between 37.8–40.35° N and 0.77–4.91° E with a distance between samples of 18 km (Fig. 2). This spatial resolution allows us to resolve the mesoscale structures, from 50 to 100 km, in the study area (Pinot et al. 2002). In 2011, 3 cruises were conducted in May, June and July, coinciding with the pre-onset, the peak and the end of the spawning activity, respectively. During 2012–2014, the oceanographic cruises were carried out from the end of June until the beginning of July, covering the peak of the spawning season. The number of stations analyzed and the dates on which the campaigns were carried out are presented in Table 1.

Ichthyoplankton samples were collected using Bongo 90 nets equipped with a mesh of 500 µm at speeds around 2 knots, with towing lasting for 8–10 min. The fishing depth was between 20 and 30 m, coinciding with the depth of the thermocline in the area during summer. In each network, HYDROBIOS flowmeters were installed to calculate the volume of water filtered in each fishing operation and a depth gauge to determine the maximum depth reached. The samples were immediately preserved with 4% formaldehyde in seawater. In addition to the ichthyoplankton samplings, vertical profiles of conductivity, temperature and pressure were recorded at each station using an SBE911 + CTD. Salinity was calibrated using International Association for the Physical Sciences of the Oceans standard seawater. New variables were calculated, derived from CTD measurements: 'smixture' and 'residualtemp'. The 'smixture' was calculated from the average salinity in the mixing layer, the ocean region adjacent to the air–sea interface, where density is fairly uniform, and extending from the surface of the ocean to the pycnocline. The 'residualtemp' was estimated using a generalized additive model (GAM), from the temperature residuals against day of the year (DOY) and position. Positive values indicate

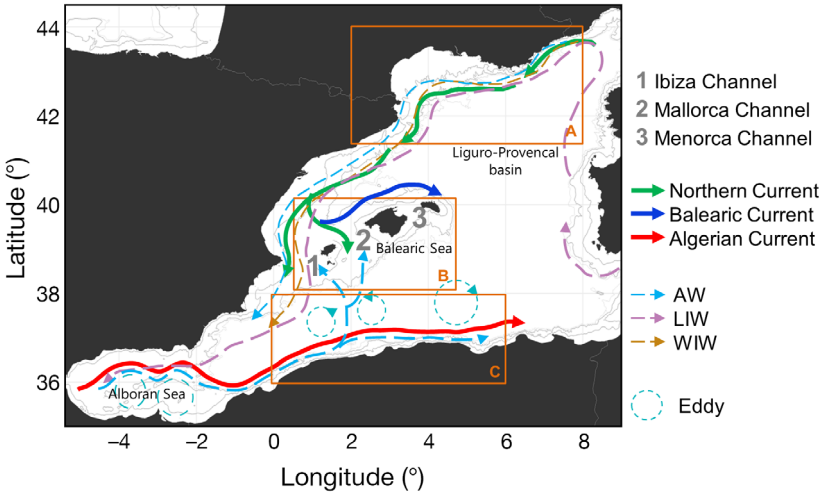

Fig. 1. Western Mediterranean circulation and study area. The Mallorca, Ibiza and Menorca channels are shown. The Algerian, Northern and Balearic Currents are indicated by thick arrows, and principal water masses (AW: Atlantic Water; LIW: Levantine Intermediate Water; WIW: Western Intermediate Water) and recurrent eddies are indicated by dashed arrows. Isobaths at 200, 1500 and 2000 m are shown. The study areas are highlighted in orange boxes: (A) Gulf of Lion, (B) sampling area in the Balearic Sea and (C) Algerian basin

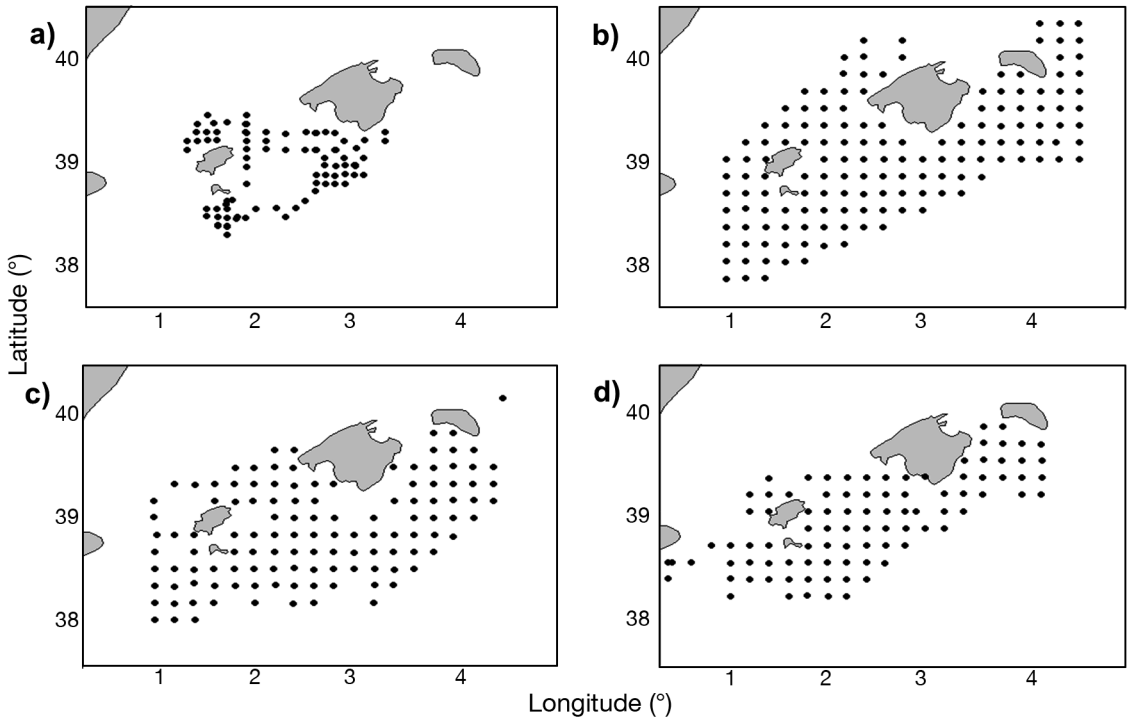

Fig. 2. Sampling mesh for oceanographic cruises conducted in the Balearic Sea in (a) 2011 (n = 3 cruises), (b) 2012, (c) 2013, (d) 2014. See Fig. 1 for details of the study area

Table 1. Ichthyoplankton oceanographic fishing cruises used for statistical analysis. Dates are given as d/mo/yr

Cruise	Year	Start date	Finish date	No. of stations analyzed
BF0511; BF0611; BF0711	2011	14/05/2011	17/07/2011	88
ATAME0612	2012	21/06/2012	13/07/2012	148
BF0613	2013	20/06/2013	10/07/2013	120
BF0614	2014	13/06/2014	03/07/2014	91

locations where water temperature is above average and negative values indicate temperatures below average, given the location and time of the year. We followed this criterion because the temperature in the mixed layer was correlated with the sampling date.

2.2. FSLEs as a proxy of mixing activity

FSLEs were originally introduced in dynamical system theory to characterize the mean growth of non-infinitesimal perturbations in turbulent flows (Aurell et al. 1997). The concept of the FSLE, based on the separation distances between pairs of fluid particle trajectories, was then further applied in the oceanographic context as a measure of dispersion, and thus of stirring and mixing (Lacorata et al. 2001), as well as to unveil dynamical structures that act as transport barriers (Boffetta et al. 2001, d'Ovidio et al. 2004).

The largest Lyapunov values occur along characteristic lines, called Lagrangian coherent structures (LCSs; Hernández-Carrasco et al. 2011, Bettencourt et al. 2012), which act as transport barriers, allowing a proper identification of fronts, eddies and filaments. Since LCSs cannot be crossed by particle trajectories, these structures strongly constrain and determine fluid motion, helping to analyze from a quantitative perspective how ocean transport is organized. The combined action of transporting, stretching and folding of fluid elements by LCS, termed 'stirring', allows the mixing process to take place. To illustrate the connection between LCS and mixing processes, Fig. 3 shows the evolution by the marine flow of 2 fluid parcels with different dyes. First, the 2 fluid elements containing different dyes (black and white) are transported over large distances (Fig. 3). The dye patches are then stretched into long filaments along the attracting LCSs (red line) identified as maximum values of backward in

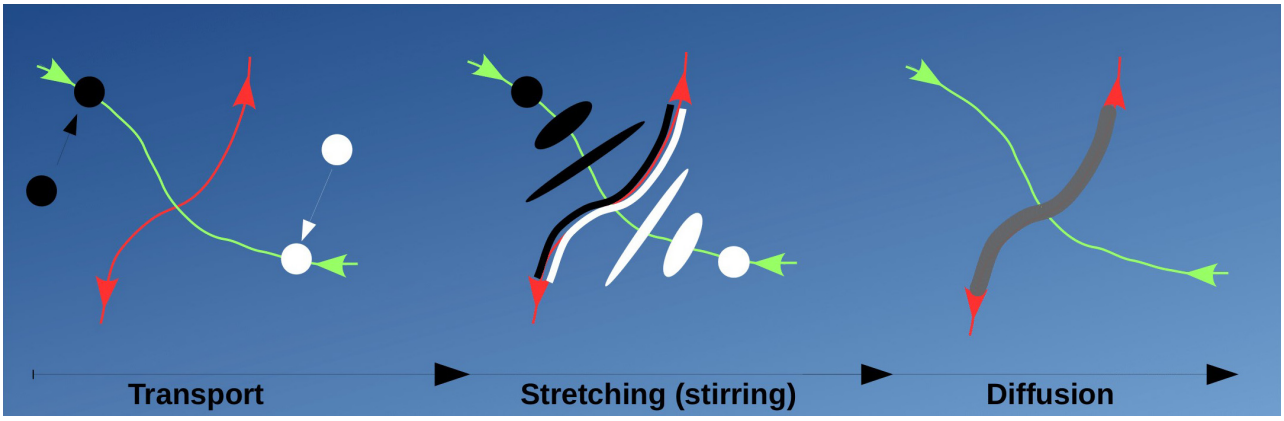

Fig. 3. Role of Lagrangian coherent structures (LCSs) in transport and stretching ('stirring') followed by diffusive mixing. Two patches of different dye (white and black) are stirred by the marine flow: fluid parcels with different dyes are transported over long distances (left panel), stretched along the repelling and attracting LCSs (in green and red) given by the ridges of the finite size Lyapunov exponent (FSLE) field and brought in close contact (middle panel). Once chaotic stirring has stretched the dye to sufficiently small length scales, diffusion dominates and mixing of the dyes occurs (grey tracer) (right panel)

time FSLEs and brought in close contact (Fig. 3). Finally, once LCSs have stretched the dye patches, creating high gradients on sufficiently small length scales, diffusion dominates and the mixing of both dyes occurs, resulting in a gray patch (Fig. 3) (Ottino 1990, Neufeld & Hernández-García 2009).

In 2-dimensional flows, the FSLEs are obtained by computing the time τ, at which 2 particles, one initially centered at location (x,y) and the other one separated by a specific distance δ_0, are advected in the fluid flow up to a given final distance of separation δ_f. The FSLE is given at position (x,y) and time t by:

$$\mathrm{FSLE}(x,y,t,\delta_0,\delta_f)=\frac{1}{\tau}\ln\frac{\delta_f}{\delta_0} \quad (1)$$

where $\delta_0 = \delta$ and $\delta_f = r\delta_0$, with r being the amplification factor of separation, that in order to properly obtain the LCS is chosen sufficiently large (e.g. $r >> 2$) to adequately distinguish ridges (extrema) of the FSLE field.

FSLEs can be obtained from particle trajectories advected forward or backward in time. In this work, we computed the FSLEs backward in time. However, given that in incompressible flows the forward and backward FSLEs are related by temporal and spatial shifts (Haller & Sapsis 2011), and that we are interested in temporal and spatial averages over relatively large scales, we do not expect significant differences between backward and forward exponents to estimate the mixing quantifiers used here. This equivalence between averaged forward and backward FSLEs to estimate mixing activity was also explicitly shown by d'Ovidio et al. (2004) for a marine flow.

FSLEs were then obtained by computing fluid particle trajectories in daily absolute geostrophic surface currents derived from sea level anomalies and regional mean dynamic topography Ssalto/Duacs multimission altimeter regional L4 product at 1/8° spatial resolution, released in 2016 by AVISO+ (https://www.aviso.altimetry.fr) and currently distributed by the Copernicus Marine Environment Monitoring Service (CMEMS; http://marine.copernicus.eu/). Following the algorithm described by Hernández-Carrasco et al. (2011), the integration of particle trajectories was carried out using a step-size adapting fourth/fifth-order Runge-Kutta scheme in order to reduce the numerical diffusion and bilinear interpolation in space and linear in time. Note that in this work, we were interested in analyzing the flow properties rather than tracking larval motion. As a consequence, we computed trajectories of neutrally buoyant particles, simulating fluid particles. A diffusion term was not included in the Lagrangian model, as Lagrangian dynamics are not significantly affected (Hernández-Carrasco et al. 2011).

2.3. Statistical analysis

The methodological approach includes 2 steps: the identification of the spatial scale at which the relationship between FSLEs and the probability of presence of larvae emerge, and the evaluation of the potential improvement of the models when FSLEs are included. We used same statistical methodology in all steps, presence probabilities are modeled applying GAMs with binomial distributions (Wood 2006), where ≥1 larva is indicated as 1 and represents presence, and 0 indicates absences, in the sam-

pling stations. As model performance indicators, we used Akaike's information criterion (AIC; Akaike 1981), for which lower values are considered better, and the area under the curve (AUC; Robin et al. 2011), for which higher values are considered better. All statistical calculations were computed in R software (R Development Core Team 2008).

2.3.1. Spatial scale analysis

The presence of larvae in a specific location can be largely influenced by the spatial scales of the hydrodynamic processes occurring around that location. Therefore, one of our aims was to find the spatial scale at which the relationship between FSLEs and the probability of presence of larvae emerges. Note, however, that 3 different scales come into play in the measurement of the hydrodynamic processes in the sampling area:

(1) Eulerian spatial scale: scale given by the spatial resolution of the velocity field. This scale represents the effective scale that controls the dynamics that can be inferred by the spatial and temporal resolution of the satellite-derived geostrophic currents, in our case limited to slow (weekly) and mesoscale structures (10–100 km).

(2) Lagrangian spatial scale: scale of the dynamical structures originated by the folding and stretching of the fluid flow, which is given by the spatial resolution at which the FSLEs are calculated. One of the significant properties of FSLEs is that they are able to reveal oceanic structures below the nominal resolution of the velocity field being analyzed.

The scaling properties and robustness of the FSLEs were investigated by Hernández-Carrasco et al. (2011), who reported that the spatial resolution at which FSLEs are computed has a relevant effect on the type of dynamical features that could be identified, showing that FSLEs have typical multifractal properties. This means that FSLEs obtained at a finer resolution than the resolution of a given velocity field provide non-artificial information. In other words, through FSLEs we can capture some effects of the large-scale structures on scales which are smaller than the resolution of velocity data. This is mainly due to the capacity of the Lagrangian diagnostics to exploit the spatiotemporal variability of the velocity field by following fluid particle trajectories. Of course, all effects derived from oceanographic processes occurring at smaller scales than the measured ones cannot be reconstructed (for example the ones originating from small mixed layer eddies). In our case, we used an altimetry-derived geostrophic velocity product provided by CMEMS; therefore, submesoscale processes cannot be resolved, and we were only able to reconstruct the structures derived from the interaction between mesoscale geostrophic structures (10–100 km). Following the algorithm provided by Hernández-Carrasco et al. (2011), daily FSLE surface fields for the 4 years of study were computed for the Western Mediterranean. We computed daily maps of FSLEs at 2 spatial resolutions (Lagrangian spatial scale), $\delta_0 = 1/8°$ and $\delta_0 = 1/64°$, and we used an amplification factor, r, equal to 10 (see Eq. 1), to properly identify regions of maximum stretching.

(3) Smoothing scale: size of the surrounding area that could be affected by the dynamical features, which is given by the size of the averaging window used in the spatial smoothing of FSLEs around the sampling position.

To analyze the spatial scale at which the relationship between FSLEs and the probability of larval presence emerges, we followed an approach that has already been applied in previous studies focused on scale analysis in pelagic environments (Alvarez-Berastegui et al. 2014, Schneider 2018).

(1) To compute the spatial smoothing of FSLEs, we used a round polygon with different sizes that determine the scales (α), generating a variable called $FSLE_\alpha$. Variations in the spatial scale were performed using a kernel matrix (circular convolution matrix, using 1 and NA [not available, i.e. missing value] to create a circular form). This procedure consists in the following steps: (i) we used a square matrix with odd dimensions, and placed the center element of the kernel matrix over the source pixel. (ii) Each value of the kernel was then multiplied by the corresponding pixel (convolution); (iii) the resulting multiplied values were summed; and (iv) the resulting value from (iii) was returned as the new value of the central pixel. The source pixel was then replaced with a weighted sum of itself and surrounding pixels obtained from the convolution kernel application. The output is placed in the destination pixel value. This process is repeated across the entire image. The reference delta was 0.125° (9 × 9 pixels, ca. 13 km), and the matrix was incremented by 0.125° until 1°.

(2) To assess the power of FSLEs to predict the habitats of larval tuna, we evaluated the relationship between daily $FSLE_\alpha$ and the probability of the presence of bluefin tuna larvae using the formula:

$$Lpp = s(\mathrm{FSLE}_\alpha, k = 3) + \varepsilon \quad (2)$$

where *Lpp* is the larval presence probability; *s* is a smooth function; *k* is the number of knots for the *s*

function, and ε is the error term. The objective is to identify the best spatial smoothing scale, comparing the performance of the different outputs obtained from modeling the *Lpp* against daily $FSLE_{\alpha}$ (Eq. 2), and following the statistical criteria mentioned at the beginning. The FSLE smoothed at the spatial window that better accounts for larval presence is termed 'FSLE-optimal smoothed' (FSLEos). Note that we used daily fields of the FSLEos to be assigned to each sampling location and time. Furthermore, we calculated the time average of FSLEos over the bluefin tuna spawning season in the 4 yr of study. The aim is to show the hydrodynamic singularities of the Balearic Sea with respect to other regions in the Western Mediterranean Sea.

2.3.2. FSLE as a habitat descriptor variable

To evaluate of the potential improvement of the models when FSLE is included, the first step explored the potential correlation between the 'basic' and 'environmental hydrographic' variables with FSLEos, as an additional variable accounting for differences in dynamical conditions, applying Pearson's correlation coefficient; we then checked that there was no correlation between them. These variables were selected from previous studies in the area (Reglero et al. 2012).

The evaluation was addressed by comparing the results of 3 different models to explain larval presence from a binomial distribution. The first model, considered the 'basic' model, included basic standardization variables; time of day ('hour'), filtered volume during fishing ('volume'), interannual variability ('year'), day of the year ('DOY'). A second model, denoted 'hydrographic', also included habitat environmental variables: average salinity in the mixing layer ('smixture') and the variation in temperature of each day at the sampling station with respect to the average value of the temperature of the year ('residualtemp'). The third model, the 'FSLEmodel', also included the FSLEos. The maximum number of smoothing oscillations in the GAM evaluations was set to 3 in order to avoid overfitting, except for the time of day variable, which was assigned to 7. To assess the effects of the different variables on the presence of larvae, a variable selection approach was applied on the basis of variable significance ($p \leq 0.05$) and the lower AIC.

The selection of the presence probabilities in the framework of this study was made for various reasons. Firstly, the data set of larval abundances is strongly skewed to low values, making the binomial distribution adequate to explore relations with environmental variables. This is the same approach applied in the framework of the International Commission for the Conservation of Atlantic Tunas (ICCAT), where larval abundances are assessed through delta-log normal models, in which presence probabilities play a main role (Ingram et al. 2017, Alvarez-Berastegui et al. 2021). Secondly, it is the most relevant statistical parameter used today to identify habitats of tuna larvae in the study area, not only for bluefin tuna but also for other tuna species (Alvarez-Berastegui et al. 2016, 2018)

3. RESULTS

3.1. Optimal spatial scale of FSLE describing mesoscale mixing

We compared 2 different Lagrangian scales, i.e. 1/8° (same as the velocity grid) and 1/64°. While the structures observed in the FSLE field at δ_0 = 1/8° (Fig. 4a) are also captured in the FSLE at δ_0 = 1/64° (Fig. 4b), new structures appear in areas previously regarded as almost inactive. While the FSLE computed at 1/8° (the same resolution as the velocity field) identifies the main large structures, the computation of FSLE at 1/64° shows new structures in areas previously regarded as almost inactive, such as smaller eddies or thin filament-like structures originated by the twist and fold of the mesoscale eddies. Close-ups of the sampling area (Fig. 4c,d) clearly show that FSLE is able to unveil subgrid filament-like structures when increasing the spatial resolution of the FSLE field below the spatial resolution of the velocity field, that is, using an initial pair separation of $\delta_0 < 1/8°$. The origin of these small-scale filaments is the stretching and folding of fluid elements produced in the interaction between large eddies. This suggests that the small-scale features captured from FSLE computed at finer resolution provide an improved quantification of the local mixing activity.

We then further analyzed the spatial scale around the sampling location, at which the presence of larvae is strongly related to the mixing process. The spatial smoothing of the FSLE was computed for 8 different scales, α. The AUC and AIC of the GAMs computed with the finest FSLE (δ_0 = 1/64°) at the different scales, α, are presented in a graphical scalogram (Fig. 5). According to the statistical criteria, the scale of 0.625° proved to be the optimal spatial scale, i.e. with the lowest AIC and the highest AUC, and

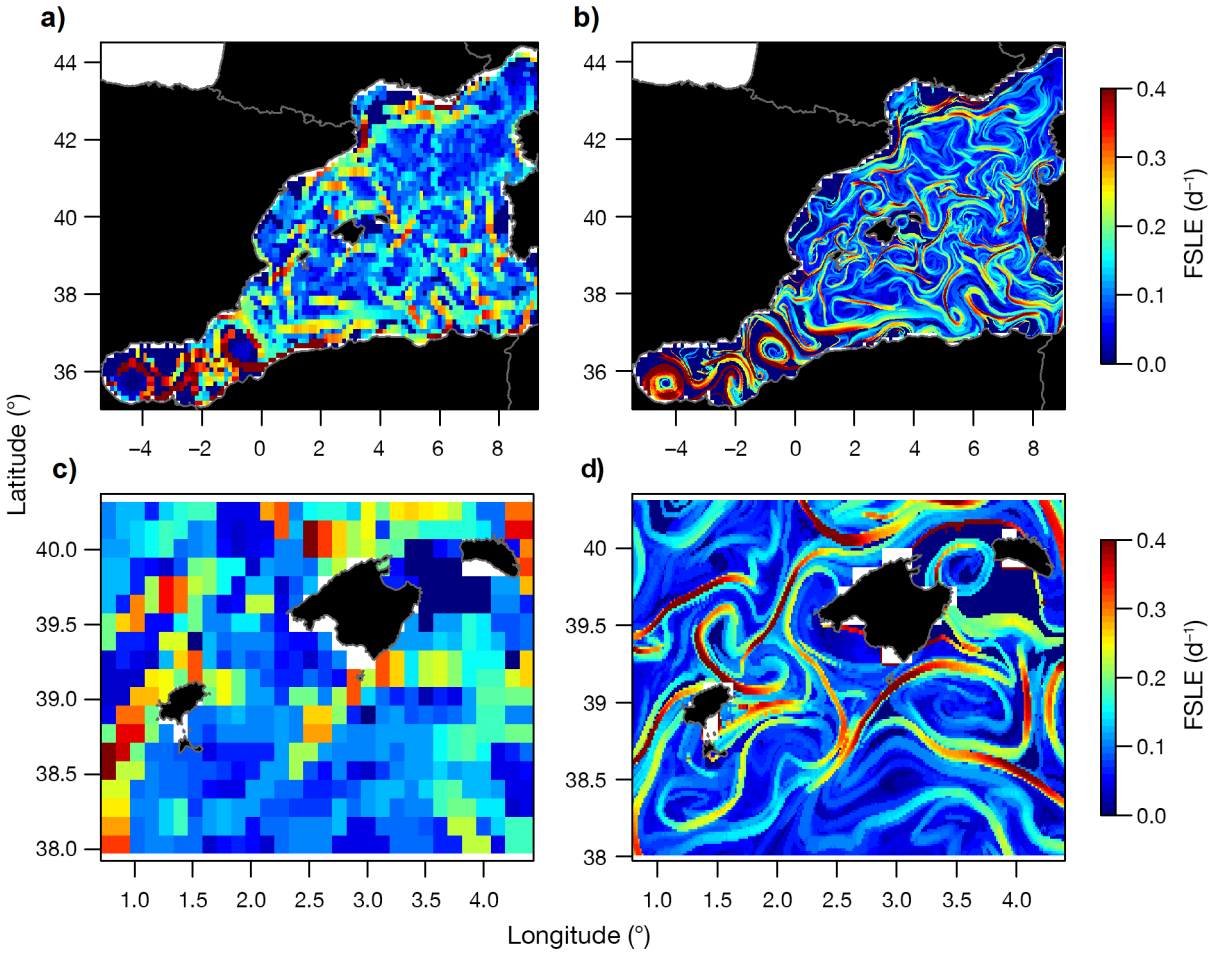

Fig. 4. Snapshots of finite size Lyapunov exponent (FSLE) backward fields for 14 May 2012, computed at 2 different spatial resolutions (a) 1/8° and (b) 1/64°. (c,d) Close-ups of the Balearic Sea from panels (a) and (b), respectively

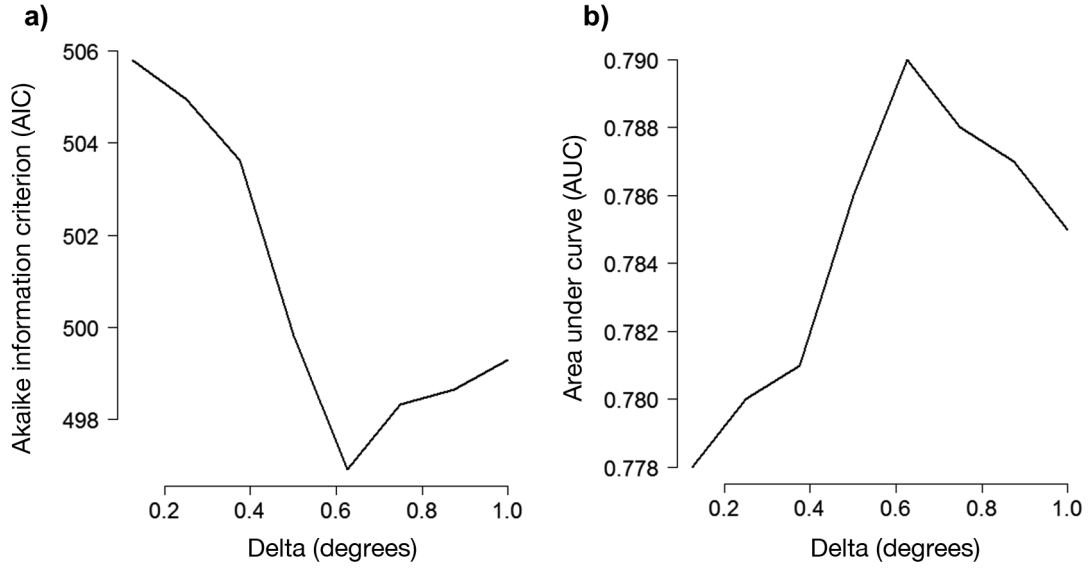

Fig. 5. Scalograms showing the change in model performance for the probability of bluefin tuna larval presence at different spatial scales for (a) Akaike's information criterion (AIC, where lower values are better) and (b) area under the curve (AUC, where higher values are better)

therefore the FSLE smoothed at this scale was chosen as the optimal FSLE (FSLEos) for the remaining analyses. To illustrate the difference between the optimal and the original scales in the FSLE computations, Fig. 6 displays both snapshots for 15 June 2011 with the original resolution of 1/64° (Fig. 6a) and the FSLEos with α = 0.625° (Fig. 6b). While it is possible to identify the mesoscale structures governing the flow dynamics, such as filaments, fronts and eddies in the instantaneous maps of FSLE (at a given time) at higher resolution, the FSLEos map shows the surrounding effect of mixing restricted by areas.

Table 2. Summary of generalized additive models of bluefin tuna larvae presence probability (Lpp): (1) initial model configuration; (2) model configuration after variable selection process. AIC: Akaike's information criterion; AUC: area under the curve; DOY: day of year; smixture: average salinity in the mixing layer; residualtemp: average value of the temperature of the year; FSLEos: optimal-smoothed finite size Lyapunov exponent

Model group	Model variables	AIC	Delta AIC	AUC
Basic model	(1) Lpp = volume + DOY + hour + year	516.856	0	0.758
	(2) Lpp = DOY + year	514.120	2.736	0.756
Hydrographic model	(1) Lpp = DOY + year + smixture + residualtemp	506.639	10.218	0.774
	(2) Lpp = DOY + year + residualtemp	508.473	8.384	0.769
FSLE model	(1) Lpp = DOY + year + residualtemp + FSLEos	496.911	19.946	0.790

3.2. Predictive power of mixing activity in the larval habitat

The 3 models tested to evaluate of the potential improvement present different performances (Table 2). The 'basic' model shows the lowest performance (highest AIC and lowest AUC) and retained the variables DOY and year, and the 'hydrographic' model retained DOY, year and residualtemp, showing the relevance of the latter variable. The 'FSLE-model' retained DOY, year, residualtemp and FSLEos. In this last model, smixture was excluded, as it had no significant effect on larval presence. This demonstrates that FSLEos has a higher predicting power than salinity. Regarding the functional responses of the variables included in the FSLE model, both DOY and the residual temperature have a positive response (Fig. 7a,d) to the presence of larvae, while FSLEos shows a dome-shaped effect on larval presence, with a maximum at moderated values of 0.1 d^{-1} (Fig. 7c). The response of the binomial model on larval presence probabilities classified for real presences and real absences (Fig. 8) shows that the FSLE model provides high probability values for stations where larvae are present in the fishing tows and a wide range of probability values for stations with no larval catches. This confirms that FSLEos improves the predictive power of the larval presence model.

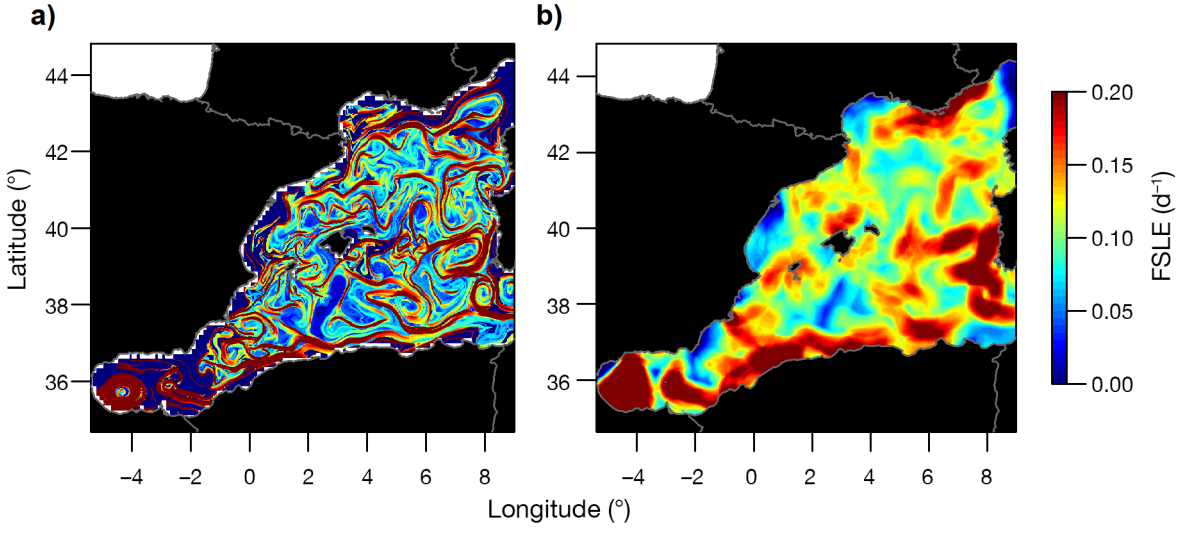

Fig. 6. Snapshots of the finite size Lyapunov exponent (FSLE) field for 15 June 2011, corresponding to (a) original FSLE computed at δ_f = 1/64° and (b) the 'optimal smoothed' FSLE (FSLEos) at the optimal scale of 0.625°

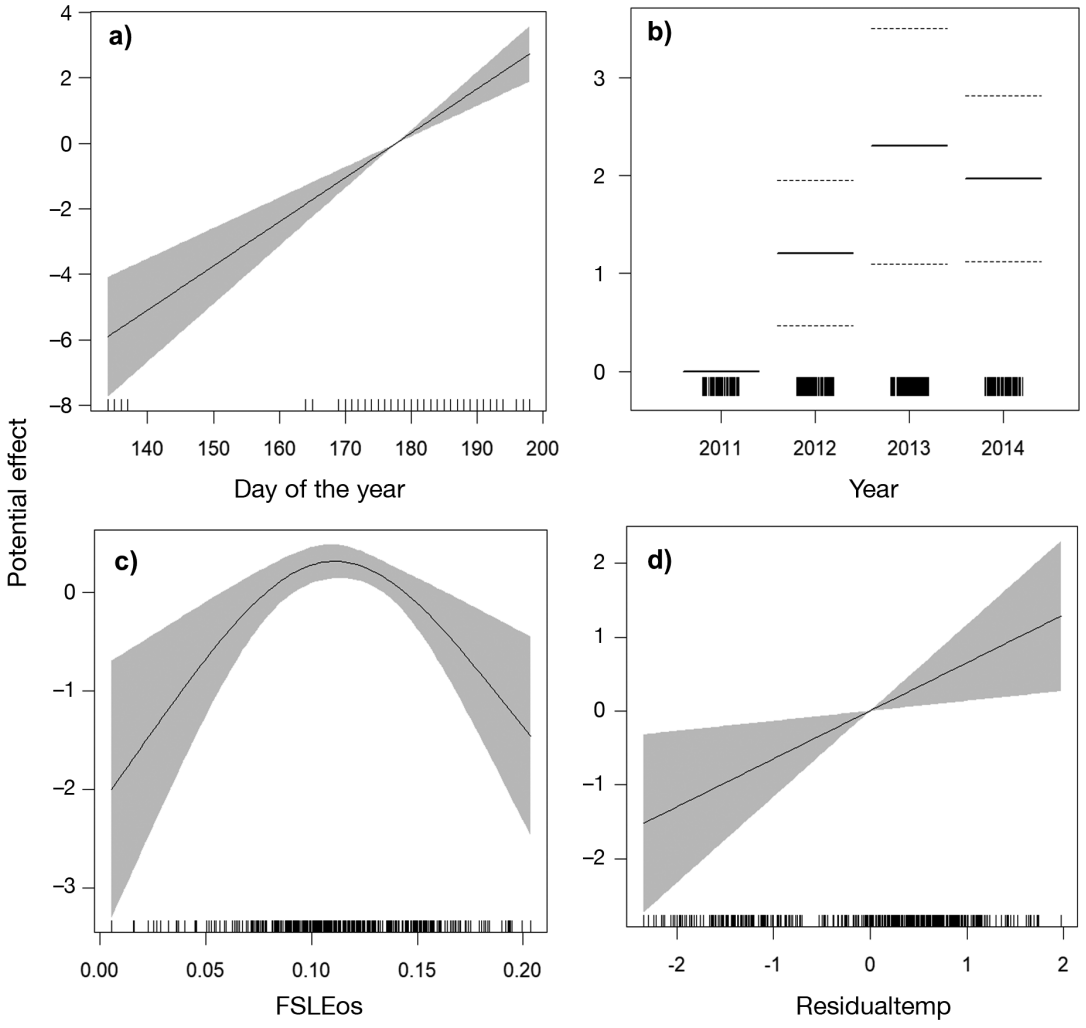

Fig. 7. Response effects of the larval presence probabilities of the generalized additive model ('FSLEmodel') for the variables: (a) day of the year, (b) year, (c) optimal-smoothed finite size Lyapunov exponent (FSLEos) and (d) residual temperature (residualtemp). The black lines on the *x*-axis represent the number of samples we found in each value for the different variables. The black line corresponds to the mean and the gray band is the standard deviation

3.3. Spatial and temporal hydrodynamic singularities during the spawning season

Instantaneous maps of FSLEs (at given time) have a significant signature of short-lived fast processes and are adequate to extract LCS, but in this research, we were also interested in slower processes at larger scales. We therefore took time averages of FSLEs over the spawning periods, in order to select the low-frequency, large-scale signal. In this way, we can easily characterize regions in the Western Mediterranean with different horizontal mixing activity; areas with larger values of FSLEos are identified as zones with more persistent horizontal mixing. In this study, the temporal averaged FSLEos over June and July (the spawning season) for the 4 sampling years showed a predominant and persistent effect of mixing restricted by areas. We found high values of mixing activity in the Alboran Sea, in the eastern Gulf of Lion and in the Algerian basin (Fig. 9). Large FSLEos values (≥ 0.2 d^{-1}) were obtained in this basin as the result of the mesoscale activity induced by the presence of the intense vortices located in the Alboran Sea and their associated frontal dynamics, and the continuous detachment of eddies formed by flow–topography interaction in the Algerian Current. The Balearic Islands and the north of the Algero-Provençal basin present medium-low FSLE values (<0.1 d^{-1}). This high spatial variability of averaged FSLE reveals the Balearic basin as a particular hydrodynamic region characterized by low values of FSLE, as compared to the rest of the Western Mediterranean, dur-

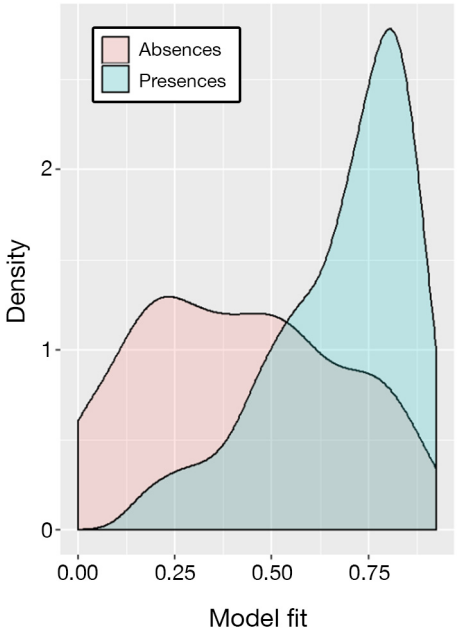

Fig. 8. Finite size Lyapunov exponent (FSLE) model predictions of larval presence probabilities for the study data set (blue: predictions for samples with larvae presence in the fishing tow; pink: prediction probabilities for stations with no larvae catches)

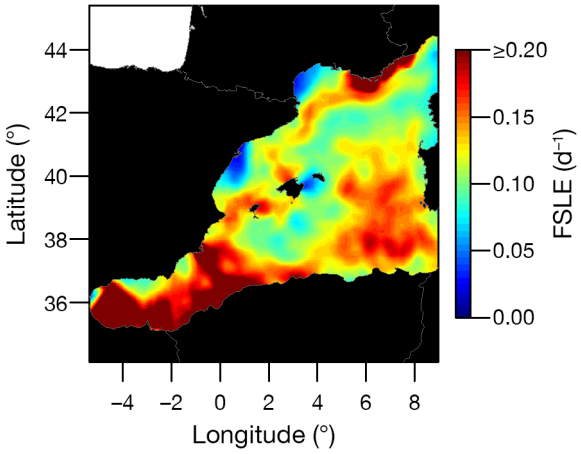

Fig. 9. Optimal-smoothed finite size Lyapunov exponent (FSLEos) mean values in the study area during the bluefin tuna spawning season (June and July) for the 2011–2014 period

ing the spawning period. This result suggests that mild mixing activity favors larval habitats.

Another convenient quantity used to characterize mixing in a prescribed geographical region R was introduced by d'Ovidio et al. (2004), which is simply the spatial average of the FSLE over that region at a given time, denoted by $< \mathrm{FSLE}(x,y,t) >_R$. This allows further investigating the temporal variability of the mixing activity in the different regions of the Western Mediterranean. In this way, mixing activity was also assessed by spatially averaging the FSLEs over the different regions in the years 2011–2014. The analyzed regions were: the Western Mediterranean Sea, the Gulf of Lion (Fig. 1, box A), the Algerian coastal basin (Fig. 1, box C) and the Balearic Sea (Fig. 1, box B). These regions were selected based on their particular hydrodynamical characteristics. The Balearic Sea area was determined by the *in situ* sampling grid area for the study years. We selected the other 2 areas following hydrographic criteria. Both regions are characterized by well-known hydrographic features. In particular, they are characterized by the presence of boundary currents, one of the major mesoscale features of the Western Mediterranean. The Gulf of Lion area includes the Northern Current (Mediterranean waters), and the Algerian basin includes the Algerian Current (Atlantic waters). We use rectangular shapes as they naturally cover the hydrographic areas of interest. The use of more complex shapes should not change the results. Finally, the resulting time series were compared between these areas, including the seasonal signal and focusing on the regional differences the FSLEs during the spawning season. Spatial averages of FSLE values for every day during the 4 yr (2011–2014) of data are shown in Fig. 10. It is worth noting that the mixing intensity, as compared to the averaged FSLE values over the Western Mediterranean basin, is typically larger in the Gulf of Lion, likely due to the intensification of the Northern Current, and in the Algerian basin, caused by the large eddy activity associated with the Algerian Current, while lower FSLE values are clearly identified over the Balearic Sea in comparison to the other study regions. Furthermore, the mean mixing activity does not show a seasonal signal over the Western Mediterranean, nor over the Algerian basin, and only slightly over the Gulf of Lion. However, the Balearic region shows clear seasonal variability with maximum values in autumn or spring and minimum values (around 0.11 d^{-1}) in summer, in particular during the months of the spawning period (June and July). This spatial and temporal consistency in the low mixing values and the high presence of larvae strongly suggests that the ocean dynamics could play an important role in the shaping of the spawning habitat area of the bluefin tuna. We found additional characteristic scales of variability at higher frequencies (around 3 wk for the Algerian basin and the Gulf of Lion and around 6 wk in the Balearic Sea and in the Western Mediterranean basin), with no relationship to the presence of larvae.

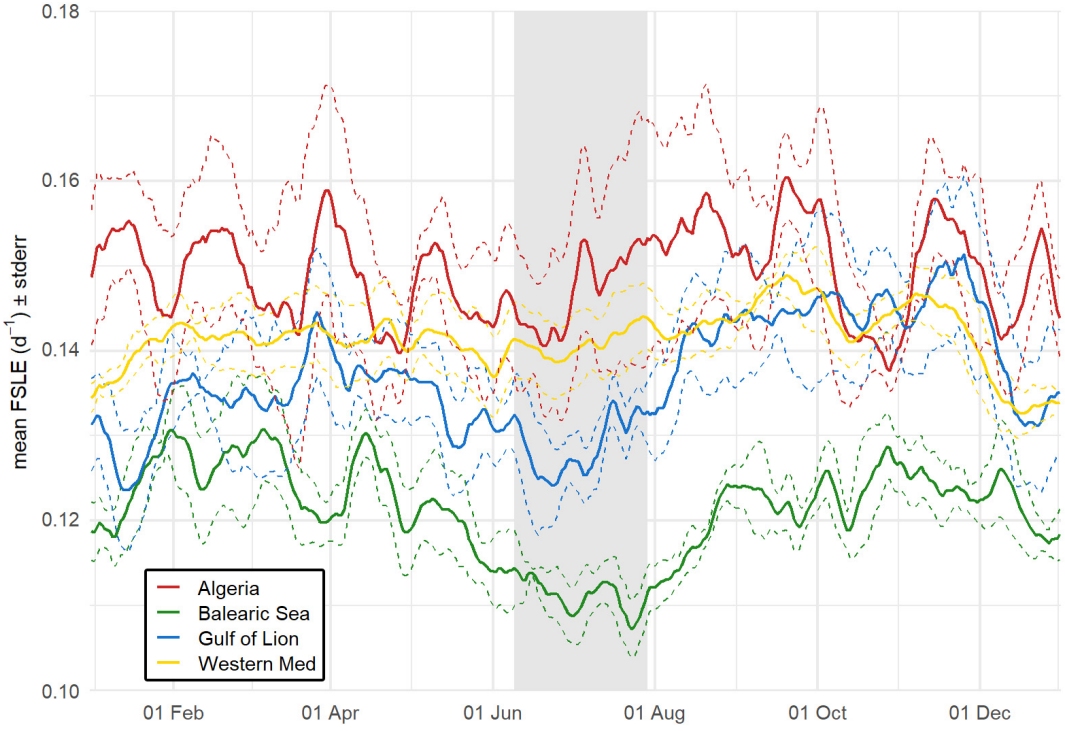

Fig. 10. Time series (2011–2014) of the finite size Lyapunov exponent (FSLE) (at 1/64°) spatial average (solid line) and the standard error (stderr) (dashed line) over the Algerian basin, Balearic Sea, Gulf of Lion and the Western Mediterranean Sea. Time range highlighted in grey shows the bluefin tuna spawning season (Reglero et al. 2012)

4. DISCUSSION

In this work, we explored how sea surface mixing activity, parameterized from FSLEs, provides new information on the environmental characteristics that define Atlantic bluefin larval habitats in the Western Mediterranean. On one hand, through spatial analysis, we revealed the scale of observation that maximizes the information regarding the spatial distribution of these habitats, i.e. 0.625° (FSLEos), and the particularities of the mixing activity in the spawning ground at the basin scale. On the other hand, and through temporal analysis, we showed that surface mixing activity in the Balearic Sea area during the spawning season (June and July) is lower than the general values at the scale of the Western Mediterranean basin. These results suggest that this hydrographic characteristic may be influential on the spatial–temporal distribution of the spawning sites. Our findings shed new light on how surface hydrodynamics affect the ecology of early life stages of bluefin tuna in an area where the relevance of mesoscale features, such as eddies and fronts, on larval distributions have been reported (Alemany et al. 2010, Reglero et al. 2012, Alvarez-Berastegui et al. 2014, Druon et al. 2021), but where the role of sea surface mixing was not examined. Investigating whether these results are consistent with other species and other areas could provide helpful advances in the discipline of pelagic seascape ecology, focused on disentangling how the spatial structure of the pelagic realm affects the ecology of the species (Alvarez-Berastegui et al. 2014, Pittman 2018).

One of the main findings of our study is that the presence of bluefin tuna larvae is not correlated with high values of FSLEs, which identify the presence of LCSs (Hernández-Carrasco et al. 2011, Bettencourt et al. 2012), but is correlated with areas where FSLE values are low/moderate (i.e. mild mixing). The FSLEos values at which the occurrence of larvae were most probable were around 0.1 d^{-1} and correspond to medium-low levels of sea surface mixing (Hernández-Carrasco et al. 2012). This pattern of higher probability of larval occurrences at moderate turbulence is consistent with previous results showing that strong turbulence has a negative effect on larvae by disaggregating food and larvae patches (Saville 1965, Peterman & Bradford 1987) and on recruitment (Lasker 1981a, Mais 1981). This is consistent with both classical theory, and evidences that

fitness of early life stages is maximized at intermediate values of mixing activity following the OEW hypothesis (Cury & Roy 1989). The OEW was proposed to explain the recruitment process on the basis of a trade-off between physical and biological constraints (i.e. food availability, predator presence). Evidence of the OEW has been shown in several studies over regional scales, particularly in small pelagic fish and upwelling systems (e.g. Guisande et al. 2001, Diankha et al. 2018), while never, to our knowledge, at such small scales as we have shown here. Also, the 'stable ocean' hypothesis suggests that high turbulence processes in the euphotic layer can increase larval mortality by reducing the availability of their planktonic prey (Lasker 1975, 1978, 1981b).

The established mechanistic role of the flow structures identified by LCS, i.e. fronts, eddies and filaments of high turbulent mixing, is regulating primary production through upwelling and aggregating processes (Lévy et al. 2018, Hernández-Carrasco et al. 2018). This generates strong dynamical interfaces identified as hot spots of marine food and therefore a target for predators (Tew Kai et al. 2009, Abrahms et al. 2018). The fitness of bluefin tuna during the early life stages could therefore be benefited by hydrodynamic environments associated with low to moderate FSLE values, that is in the absence of intense LCS which occurs in the Balearic Sea in comparison to other areas in the Western Mediterranean. This agrees with identified strategies of bluefin tuna larvae, that occupy areas spatially distributed to avoid predation from species such *Pelagia noctiluca* ephyrae (Ottmann et al. 2021) and for which cannibalistic strategies seem to play a key role for survival strategies (Reglero et al. 2011, Uriarte et al. 2019).

At a regional scale, our results reveal that during the time of spawning, the predominant mean values of the FSLEos in the Balearic Sea are lower (close to 0.1 d^{-1}) than in surrounding areas of the Western Mediterranean Sea (Figs. 9 & 10). It is known that the spawning grounds are associated with the oceanic front located in the Balearic sea generated by the mixing of the incoming Atlantic waters from the Strait of Gibraltar and the more resident Mediterranean waters (Alvarez-Berastegui et al. 2014), but these new results show that remote sensing observations parameterized through the FSLEos provide additional information to describe the environmental signals that mark the spatial distribution of adequate habitats for bluefin tuna larvae. Also, this analytic tool provides a quantitative measurement to parameterize oceanographic surface processes identifying LCSs, and therefore transport barriers, which determine the general transport template of particles in marine flows. This opens the possibility of identifying and developing new variables and ocean monitoring indicators, which are key for the integration of the hydrodynamic variability into the study of the ecology of a species (Hobday & Hartog 2014), and for the application of operational oceanography to respond to the challenges of the SDG14 and the UN's Decade of Ocean Science for sustainable development (Tintoré et al. 2019).

The FSLEos showed a higher predictive power to explain larval occurrences than salinity values in the mixed layer depth. Salinity is a proxy for the location of the front in the area and has been one of the most relevant explanatory variables used in previous studies for identifying tuna larval habitat distributions (Alemany et al. 2010, Reglero et al. 2012, Alvarez-Berastegui et al. 2014). The higher relevance of the FSLEos compared to the salinity found in this study reveals the potential of applying these metrics to improve quantitative identification of larval habitats to standardize interannual variability in larval abundances. The habitat standardization to improve larval abundance estimations is applied for the bluefin tuna population assessment models by the scientific groups of the ICCAT to assess the total allowable catch of this species and other tunas (ICCAT 2017, Ingram et al. 2017, Alvarez-Berastegui et al. 2018).

One of the limitations of the ichthyoplankton surveys is that they provide real presence of larvae when they are found in the catches, but they do not provide real absences when they are not present in the catch. The different possible scenarios are (1) probability of presence and being detected, (2) probability of presence and not being detected and (3) probability that they are not present and therefore are not detected (Steventon et al. 2005). The existence of the second case influences the capacity of downward predictive models regarding absences, and this limits the effectiveness of the binomial models to detect the real absences, as shown by the selected binomial model which included the FSLEos. This result should be considered when developing larval distribution models.

This study proves the importance of considering sea surface mixing processes when studying the early life ecology of bluefin tuna in the upper water column, and it contributes to advance the integration of environmental variability into the standardization of abundance indices used for fisheries assessment, a relevant path for the practical implementation of ecosystem-based fisheries management (Skern-Mauritzen et al. 2016). FSLE metrics could indeed

be relevant for improving knowledge of the spawning and early life stage survival of other pelagic species evolutionarily adapted to maximize opportunities provided by mesoscale processes in the upper water column, such as tuna and swordfish species, but also small pelagic fish. Further research is needed to implement these metrics in modern stock assessments and management practices.

Acknowledgements. We thank the scientists and crew participating in the BLUEFIN TUNA and ATAME (CTM2011-29525-C04-02) cruises. This study was funded by the BLUEFIN TUNA project (SOCIB and IEO joint action), the PANDORA project from the EU2020 Program (Grant Agreement No 773713), and MINECO/FEDER Project MOCCA (256RTI2018-093941-B-C31). I.H.C. acknowledges the Vicenç Mut contract funded by the Government of the Balearic Islands and the European Social Fund (ESF) Operational Programme. The multimission altimeter product was produced by Ssalto/Duacs and provided by CMEMS (http://marine.copernicus.eu).

LITERATURE CITED

Abrahms B, Scales KL, Hazen EL, Bograd SJ, Schick RS, Robinson PW, Costa DP (2018) Mesoscale activity facilitates energy gain in a top predator. Proc R Soc B 285: 20181101

Akaike H (1981) Likelihood of a model and information criteria. J Econom 16:3–14

Alemany F, Quintanilla L, Velez-Belchí P, García A and others (2010) Characterization of the spawning habitat of Atlantic bluefin tuna and related species in the Balearic Sea (western Mediterranean). Prog Oceanogr 86:21–38

Alvarez-Berastegui D (2020) Environmental variability in three major Mediterranean tuna spawning grounds: updating SST indicators for the Ecosystem Report Card. Collect Vol Sci Pap ICCAT 77:137–143

Alvarez-Berastegui D, Ciannelli L, Aparicio-Gonzalez A, Reglero P and others (2014) Spatial scale, means and gradients of hydrographic variables define pelagic seascapes of bluefin and bullet tuna spawning distribution. PLOS ONE 9:e109338

Alvarez-Berastegui D, Hidalgo M, Tugores PM, Reglero P and others (2016) Pelagic seascape ecology for operational fisheries oceanography: modelling and predicting spawning distribution of Atlantic bluefin tuna in Western Mediterranean. ICES J Mar Sci 73:1851–1862

Alvarez-Berastegui D, Saber S, Ingram GW Jr, Díaz-Barroso L and others (2018) Integrating reproductive ecology, early life dynamics and mesoscale oceanography to improve albacore tuna assessment in the Western Mediterranean. Fish Res 208:329–338

Alvarez-Berastegui D, Tugores MP, Martín M, Leyva L and others (2021) Bluefin tuna larval indices in the Balearic Archipelago for the management strategy evaluation ('Strict Update' and 'Revised Version' for 2001–2019 period). SCRS/2021/033. Collect Vol Sci Pap ICCAT 78: 323–337

Aurell E, Boffetta G, Crisanti A, Paladin G, Vulpiani A (1997) Predictability in the large: an extension of the concept of Lyapunov exponent. J Phys A Math Gen 30:1–26

Balbín R, López-Jurado JL, Flexas MM, Reglero P and others (2014) Interannual variability of the early summer circulation around the Balearic Islands: driving factors and potential effects on the marine ecosystem. J Mar Syst 138:70–81

Bettencourt JH, López C, Hernández-García E (2012) Oceanic three-dimensional Lagrangian coherent structures: a study of a mesoscale eddy in the Benguela upwelling region. Ocean Model 51:73–83

Boffetta G, Lacorata G, Redaelli G, Vulpiani A (2001) Detecting barriers to transport: a review of different techniques. Physica D 159:58–70

Capó E, Orfila A, Mason E, Ruiz S (2019) Energy conversion routes in the Western Mediterranean Sea estimated from eddy–mean flow interactions. J Phys Oceanogr 49: 247–267

Ciannelli L, Bailey K, Olsen EM (2015) Evolutionary and ecological constraints of fish spawning habitats. ICES J Mar Sci 72:285–296

Cury P, Roy C (1989) Optimal environmental window and pelagic fish recruitment success in upwelling areas. Can J Fish Aquat Sci 46:670–680

D'Ovidio F, Fernández V, Hernández-García E, López C (2004) Mixing structures in the Mediterranean Sea from finite-size Lyapunov exponents. Geophys Res Lett 31: L17203

D'Ovidio F, Isern-Fontanet J, López C, García-Ladona E, Hernández-García E (2009) Comparison between Eulerian diagnostics and the finite-size Lyapunov exponent computed from altimetry in the Algerian Basin. Deep Sea Res I 56:15–31

Diankha O, Ba A, Brehmer P, Brochier T and others (2018) Contrasted optimal environmental windows for both sardinella species in Senegalese waters. Fish Oceanogr 27: 351–365

Druon JN, Fromentin JM, Hanke AR, Arrizabalaga H and others (2016) Habitat suitability of the Atlantic bluefin tuna by size class: an ecological niche approach. Prog Oceanogr 142:30–46

Druon JN, Gascuel D, Gibin M, Zanzi A and others (2021) Mesoscale productivity fronts and local fishing opportunities in the European Seas. Fish Fish 22:1227–1247

Escudier R, Mourre B, Juza M, Tintoré J (2016) Subsurface circulation and mesoscale variability in the Algerian subbasin from altimeter-derived eddy trajectories. J Geophys Res Oceans 121:6310–6322

García-Ladona E, Castellón A, Font J, Tintoré J (1996) The Balearic current and volume transports in the Balearic basin. Oceanol Acta 19:489–497

Guisande C, Cabanas JM, Vergara AR, Riveiro I (2001) Effect of climate on recruitment success of Atlantic Iberian sardine *Sardina pilchardus*. Mar Ecol Prog Ser 223: 243–250

Haller G, Sapsis T (2011) Lagrangian coherent structures and the smallest finite-time Lyapunov exponent. Chaos 21:023115

Hernández-Carrasco I, Orfila A (2018) The role of an intense front on the connectivity of the Western Mediterranean Sea: the Cartagena-Tenes Front. J Geophys Res 123: 4398–4422

Hernández-Carrasco I, López C, Hernández-García E, Turiel A (2011) How reliable are finite-size Lyapunov exponents for the assessment of ocean dynamics? Ocean Model 36:208–218

Hernández-Carrasco I, López C, Hernández-García E, Turiel A (2012) Seasonal and regional characterization of

horizontal stirring in the global ocean. J Geophys Res 117:C10007
Hernández-Carrasco I, Orfila A, Rossi V, Garçon V (2018) Effect of small scale transport processes on phytoplankton distribution in coastal seas. Sci Rep 8:8613
Hernández-Carrasco I, Alou E, Doumont P, Cabornero A, Allen J, Orfila A (2020) Lagrangian flow effects on phytoplankton abundance and composition along filament-like structures. Prog Oceanogr 189:102469
Hobday AJ, Hartog JR (2014) Derived ocean features for dynamic ocean management. Oceanography 27:134–145
ICCAT (2017) Report of the 2017 ICCAT bluefin stock assessment meeting (Madrid, Spain, 20–28 July, 2017). www.iccat.int/Documents/Meetings/Docs/2017_BFT_ASS_REP_ENG.pdf (accessed 28 November 2019)
Ingram GW Jr, Alvarez-Berastegui D, Reglero P, Balbín R, García A, Alemany F (2017) Incorporation of habitat information in the development of indices of larval bluefin tuna (*Thunnus thynnus*) in the Western Mediterranean Sea (2001–2005 and 2012–2013). Deep Sea Res II 140: 203–211
La Violette PE, Tintoré J, Font J (1990) The surface circulation of the Balearic Sea. J Geophys Res 95:1559–1568
Lacorata G, Aurell E, Vulpiani A (2001) Drifters dispersion in the Adriatic Sea: Lagrangian data and chaotic model. Ann Geophys 19:121–129
Lasker R (1975) Fish criteria for survival of anchovy larvae: the relation between inshore chlorophyll maximum layers and successful first feeding. Fish Bull 73:453–462
Lasker R (1978) The relation between oceanographic conditions and larval anchovy food in the California Current: identification of factors contributing to recruitment failure. Rapp P-V Reùn Cons Int Explor Mer 173:212–230
Lasker R (1981a) Factors contributing to variable recruitments of the Northern anchovy (*Engraulis mordax*) in the California current: contrasting years, 1975 through 1978. Rapp P-V Réun Cons Int Explor Mer 178:375–388
Lasker R (1981b) Marine fish larvae. Morphology, ecology, and relation to fisheries. University of Washington Press, Seattle, WA
Lehahn Y, D'Ovidio F, Lévy M, Heyfetz E (2007) Stirring of the Northeast Atlantic spring bloom: a Lagrangian analysis based on multisatellite data. J Geophys Res Oceans 112:C08005
Lévy M, Franks PJS, Smith KS (2018) The role of submesoscale currents in structuring marine ecosystems. Nat Commun 9:4758
Mais KE (1981) Age-composition changes in the anchovy, *Engraulis mordax*, central population. Calif Coop Ocean Fish Invest Rep 22:82–87
Maps F, Plourde S, McQuinn IH, St-Onge-Drouin S, Lavoie D, Chassé J, Lesage V (2015) Linking acoustics and finite-time Lyapunov exponents reveals areas and mechanisms of krill aggregation within the Gulf of St. Lawrence, eastern Canada. Limnol Oceanogr 60:1965–1975
Muhling BA, Reglero P, Ciannelli L, Alvarez-Berastegui D, Alemany F, Lamkin JT, Roffer MA (2013) Comparison between environmental characteristics of larval bluefin tuna *Thunnus thynnus* habitat in the Gulf of Mexico and western Mediterranean Sea. Mar Ecol Prog Ser 486: 257–276
Muhling BA, Lamkin JT, Alemany F, García A and others (2017) Reproduction and larval biology in tunas, and the importance of restricted area spawning grounds. Rev Fish Biol Fish 27:697–732
Neufeld Z, Hernández-García E (2009) Chemical and biological processes in fluid flows: a dynamical systems approach. Imperial College Press, London
Ottino JM (1990) Mixing, chaotic advection, and turbulence. Annu Rev Fluid Mech 22:207–253
Ottmann D, Fiksen Ø, Martín M, Alemany F, Prieto L, Alvarez-Berastegui D, Reglero P (2021) Spawning site distribution of a bluefin tuna reduces jellyfish predation on early life stages. Limnol Oceanogr 66:3669–3681
Peterman RM, Bradford MJ (1987) Wind speed and mortality rate of a marine fish, the northern anchovy (*Engraulis mordax*). Science 235:354–357
Pinot JM, Tintoré J, Gomis D (1994) Quasi-synoptic mesoscale variability in the Balearic Sea. Deep Sea Res I 41:897–914
Pinot JM, Tintoré J, Gomis D (1995) Multivariate analysis of the surface circulation in the Balearic Sea. Prog Oceanogr 36:343–344
Pinot JM, López-Jurado JL, Riera M (2002) The CANALES experiment (1996–1998). Interannual, seasonal, and mesoscale variability of the circulation in the Balearic Channels. Prog Oceanogr 55:335–370
Pittman SJ (2018) Seascape ecology. Wiley Blackwell, Hoboken, NJ
Porch CE, Bonhommeau S, Diaz GA, Haritz A, Melvin G (2019) The journey from overfishing to sustainability for Atlantic bluefin tuna, *Thunnus thynnus*. In: Block BA (ed) The future of bluefin tunas: ecology, fisheries management, and conservation. Johns Hopkins University Press, Baltimore, MD, p 3–44
R Development Core Team (2008) R: a language and environment for statistical computing. R Foundation for Statistical Computing, Vienna
Reglero P, Urtizberea A, Torres AP, Alemany F, Fiksen Ø (2011) Cannibalism among size classes of larvae may be a substantial mortality component in tuna. Mar Ecol Prog Ser 433:205–219
Reglero P, Ciannelli L, Alvarez-Berastegui D, Balbín R, López-Jurado JL, Alemany F (2012) Geographically and environmentally driven spawning distributions of tuna species in the western Mediterranean Sea. Mar Ecol Prog Ser 463:273–284
Reglero P, Ortega A, Balbín R, Abascal FJ and others (2018) Atlantic bluefin tuna spawn at suboptimal temperatures for their offspring. Proc R Soc B 285:20171405
Reglero P, Balbín R, Abascal F, Medina A and others (2019) Pelagic habitat and offspring survival in the eastern stock of Atlantic bluefin tuna. ICES J Mar Sci 76:549–558
Robin X, Turck N, Hainard A, Tiberti N, Lisacek F, Sanchez JC, Müller M (2011) pROC: an open-source package for R and S+ to analyze and compare ROC curves. BMC Bioinformatics 12:77
Rooker JR, Alvarado Bremer JR, Block BA, Dewar H and others (2007) Life history and stock structure of Atlantic bluefin tuna (*Thunnus thynnus*). Rev Fish Sci Aquacult 15:265–310
Salat J (1995) The interaction between the Catalan and Balearic currents in the southern Catalan Sea. Oceanol Acta 18:227–234
Saville A (1965) Factors controlling dispersal of the pelagic stages of fish and their influence on survival. Int Comm Northwest Atl Fish Spec Publ 6:335–348
Sayol JM, Orfila A, Simarro G, Lopez C, Renault L, Galan A, Conti D (2013) Sea surface transport in the Western Mediterranean Sea: a Lagrangian perspective. J Geophys Res Oceans 118:6371–6384

Scales KL, Hazen EL, Jacox MG, Castruccio F, Maxwell SM, Lewison RL, Bograd SJ (2018) Fisheries bycatch risk to marine megafauna is intensified in Lagrangian coherent structures. Proc Natl Acad Sci USA 115:7362–7367

Schneider DC (2018) Scale and scaling in seascape ecology. In: Pittman SJ (ed) Seascape ecology. Wiley Blackwell. Hoboken, NJ, p 89–188

Skern-Mauritzen M, Ottersen G, Handegard NO, Huse G, Dingsør GE, Stenseth NC, Kjesbu OS (2016) Ecosystem processes are rarely included in tactical fisheries management. Fish Fish 17:165–175

Steventon JD, Bergerud WA, Ott PK (2005) Analysis of presence/absence data when absence is uncertain (false zeroes): an example for the northern flying squirrel using SAS. Extension Note 74. British Columbia Ministry of Forests and Range, Forest Science Program, Victoria, BC

Tew Kai E, Rossi V, Sudre J, Weimerskirch H and others (2009) Top marine predators track Lagrangian coherent structures. Proc Natl Acad Sci USA 106:8245–8250

Tintoré J, Pinardi N, Álvarez-Fanjul E, Aguiar E and others (2019) Challenges for sustained observing and forecasting systems in the Mediterranean Sea. Front Mar Sci 6:568

Twiname S, Audzijonyte A, Blanchard JL, Champion C and others (2020) A cross-scale framework to support a mechanistic understanding and modelling of marine climate-driven species redistribution, from individuals to communities. Ecography 43:1764–1778

Uriarte A, Johnstone C, Laiz-Carrión R, García A and others (2019) Evidence of density-dependent cannibalism in the diet of wild Atlantic bluefin tuna larvae (*Thunnus thynnus*) of the Balearic Sea (NW Mediterranean). Fish Res 212:63–71

Wood SN (2006) Generalized additive models: an introduction with R. Chapman & Hall, Boca Raton, FL

Editorial responsibility: Myron Peck, Den Burg, The Netherlands
Reviewed by: 3 anonymous referees

Submitted: August 20, 2021
Accepted: December 13, 2021
Proofs received from author(s): February 25, 2022